Aalto University

OPEN ACCESS

This is an electronic reprint of the original article.
This reprint may differ from the original in pagination and typographic detail.

Bala, Manju; Bhogra, Anuradha; Khan, Saif A; Tripathi, Tripurari S.; Tripathi, Surya K.; Avasthi, Devesh K.; Asokan, Kandasami

Enhancement of thermoelectric power of PbTe thin films by Ag ion implantation

Published in:
Journal of Applied Physics

DOI:
10.1063/1.4984050

Published: 07/06/2017

Document Version
Publisher's PDF, also known as Version of record

Please cite the original version:
Bala, M., Bhogra, A., Khan, S. A., Tripathi, T. S., Tripathi, S. K., Avasthi, D. K., & Asokan, K. (2017). Enhancement of thermoelectric power of PbTe thin films by Ag ion implantation. *Journal of Applied Physics*, *121*(21), [215301]. https://doi.org/10.1063/1.4984050

This material is protected by copyright and other intellectual property rights, and duplication or sale of all or part of any of the repository collections is not permitted, except that material may be duplicated by you for your research use or educational purposes in electronic or print form. You must obtain permission for any other use. Electronic or print copies may not be offered, whether for sale or otherwise to anyone who is not an authorised user.

Enhancement of thermoelectric power of PbTe thin films by Ag ion implantation

Manju Bala, Anuradha Bhogra, Saif A. Khan, Tripurari S. Tripathi, Surya K. Tripathi, Devesh K. Avasthi, and Kandasami Asokan

Citation: Journal of Applied Physics **121**, 215301 (2017); doi: 10.1063/1.4984050
View online: https://doi.org/10.1063/1.4984050
View Table of Contents: http://aip.scitation.org/toc/jap/121/21
Published by the American Institute of Physics

Articles you may be interested in

Thermoelectric properties of $[Ca_2CoO_{3-\delta}][CoO_2]_{1,62}$ as a function of Co/Ca defects and Co_3O_4 inclusions
Journal of Applied Physics **121**, 215101 (2017); 10.1063/1.4984067

Observation of defect-assisted enhanced visible whispering gallery modes in ytterbium-doped ZnO microsphere
Journal of Applied Physics **121**, 213101 (2017); 10.1063/1.4984205

An effective low-temperature solution synthesis of Co-doped [0001]-oriented ZnO nanorods
Journal of Applied Physics **121**, 215102 (2017); 10.1063/1.4984314

Electron paramagnetic resonance study of MgO thin-film grown on silicon
Journal of Applied Physics **121**, 213901 (2017); 10.1063/1.4983752

Large electronic sputtering yield of nanodimensional Au thin films: Dominant role of thermal conductivity and electron phonon coupling factor
Journal of Applied Physics **121**, 095308 (2017); 10.1063/1.4977845

Non-metallic dopant modulation of conductivity in substoichiometric tantalum pentoxide: A first-principles study
Journal of Applied Physics **121**, 214102 (2017); 10.1063/1.4983850

AIP | Journal of Applied Physics SPECIAL TOPICS LEARN MORE

Enhancement of thermoelectric power of PbTe thin films by Ag ion implantation

Manju Bala,[1] Anuradha Bhogra,[1] Saif A. Khan,[1] Tripurari S. Tripathi,[2] Surya K. Tripathi,[3] Devesh K. Avasthi,[4] and Kandasami Asokan[1]
[1]*Inter-University Accelerator Centre, Aruna Asaf Ali Marg, New Delhi 110067, India*
[2]*Aalto University, Värmemansgränden 2, 02150 Esbo, Finland*
[3]*Department of Physics, Panjab University, Chandigarh 160 014, India*
[4]*Engineering and Technology, Amity University Campus, Noida 201313, India*

(Received 20 January 2017; accepted 10 May 2017; published online 1 June 2017)

Enhancement of the figure of merit (ZT) of thermoelectric materials is the topic of current research in energy studies. We report an enhancement in the thermoelectric power (TEP) of thermally evaporated PbTe thin films by low energy Ag ion implantation. This implantation results in PbTe:Ag nanocomposites. Implantations were carried out at a 130 keV Ag ion beam with ion fluences of 3×10^{15}, 1.5×10^{16}, 3×10^{16}, and 4.5×10^{16} ions/cm^2. The atomic concentrations were determined using Rutherford backscattering and found to be 1 at. %, 5 at. %, 10 at. %, and 14 at. % in the implanted PbTe films. Scanning electron microscopy images show the presence of fine cracks on the surface of as-deposited PbTe thin films that get shortened and suppressed and finally disappear at higher fluences of Ag ion implantation. The TEP measurements, from 300 K to 400 K, show ~25% enhancement in the Seebeck coefficient of the Ag ion implanted films in comparison to the pristine PbTe thin film. The synchrotron based high resolution X-ray diffraction and X-ray photoelectron spectroscopy investigations reveal the formation of Ag_2Te in the surface layer after Ag ion implantation. *Published by AIP Publishing.* [http://dx.doi.org/10.1063/1.4984050]

I. INTRODUCTION

The advancement in nanotechnology relies on the downscaling of semiconductor devices towards nanometer dimensions for better performance and lower costs. In recent years, to achieve better device performance, implantation technology is recognized as a key for introducing dopants, since diffusion of impurities generally requires very high temperatures. Ion implantation has been effectively used in semiconductor technology to modify the electrical transport properties.[1,2] Energetic ions penetrate the surface of the target (host) material and come to rest in an approximately Gaussian depth distribution. In addition to the solute profile so-introduced, the incoming ions leave a trail of damage as these ions penetrate in the material.[3] The ions while passing through the material lose their energy mainly by elastic collisions. Ion implantation thus can modify the physical, chemical, or electrical properties of the target material. The implanted species in the semiconductor can make solutions or compounds with the host material and change the charge carrier type and density. For a *p*-type dopant, a hole is created, and for an *n*-type dopant, an electron is created in the target material. This alters the local conductivity of the material. Ion implantation can be employed in thermoelectric materials as a process to produce controlled modifications to alter the lattice and charge carriers.

Thermoelectric materials convert heat (temperature differences) directly into electrical energy, and a good thermoelectric material must have high electrical conductivity (σ), high Seebeck Coefficient (S), and low thermal conductivity (κ). The efficiency of a given material to produce a thermoelectric power is governed by its "figure of merit" $ZT = S^2\sigma T/\kappa$.[4,5] For many years, the main three semiconductors known to have both low thermal conductivity and high power factor ($S^2\sigma$) have been bismuth telluride (Bi_2Te_3), lead telluride (PbTe), and silicon germanium (SiGe).[6] Among them, PbTe has proven to be a very important intermediate thermoelectric material. It crystallizes in the NaCl crystal structure with Pb atoms occupying the cation and Te forming the anionic lattice. It is a narrow gap semiconductor with a bandgap of 0.32 eV.[7] The PbTe system can be optimized for power generation applications by improving the power factor via band engineering. It can be made either *n*-type or *p*-type with appropriate dopants. Halogens are often used as n-type doping agents. $PbCl_2$, $PbBr_2$, and PbI_2 are commonly used to produce donor centers. The common p-type doping agents are Na_2Te, K_2Te, and Ag_2Te. Besides all these elements, Ag has been found to be one of the potential dopants to enhance the thermoelectric properties of PbTe. It has been reported by Heremans *et al.* that Ag doping in PbTe acts as a p-type dopant at low concentrations (<a few 10^{19} cm^{-3}) but at higher concentrations, (>10^{19} cm^{-3}), it results in n-type.[8] Enhancement in thermoelectric power through the energy barrier scattering in Ag doped PbTe was demonstrated by Martin *et al.*[9] The effect of Ag and Sb doping on the thermoelectric properties of PbTe was reported, and the maximum $ZT = 0.27$ at 723 K for $Pb_{1-x}Ag_xTe$ alloys when $x = 0.1$ was estimated.[10] Hence, Ag doping in PbTe has been proven to improve thermoelectric properties by forming PbTe:Ag nanocomposites.[11,12] Further, ZT of PbTe can also be boosted by reducing its thermal conductivity by introducing point defects, nanoscale precipitates, and mesoscale grain boundaries.[13] These act as effective scattering centers for phonons with different mean free paths, without affecting

charge carrier transport. By applying this method, the highest value of *ZT* for PbTe that has been achieved in the Na doped PbTe-SrTe system is approximately 2.2.[14]

Ion implantation can be employed in thermoelectric materials to modify their lattice thermal conductivity and charge carriers. It is used to create an implanted buried thin layer and change the properties of PbTe materials. Shen *et al.* showed that Sn^+ ion implanted PbTe can create a $Pb_{1-x}Sn_xTe$ thin layer which lowers the lattice thermal conductivity and hence improves the *ZT* of PbTe.[15] It was reported by Kato *et al.* that *n*-type PbTe implanted with 120 keV Te^+ ions shows *p*-type character at a fluence of 1×10^{16} ions/cm^2.[16] Similarly, Donnelly *et al.* reported that Sb^+ ion implantation can convert layers of *p*-type PbTe into *n*-type.[17] However, there has been no report on the effect of these implantations on the thermoelectric properties of PbTe films. The present study aims to understand the thermoelectrical properties of Ag ion implanted PbTe thin films and also the morphological, structural, and electrical modifications at different doses.

II. EXPERIMENTAL

Thin films of PbTe were deposited on quartz substrates at room temperature by the thermal evaporation method at a base pressure of $\sim 2 \times 10^{-5}$ mbar. The Ag ions were incorporated in PbTe thin films by Ag ion implantation using the Negative Ion Implanter (NII) facility available at the Inter-University Accelerator Centre (IUAC), New Delhi. The implantation was carried out at room temperature and the pressure was maintained at 10^{-4} Pa. The PbTe films were implanted with 130 keV Ag^- ions to 4 different fluences: 3×10^{15}, 1.5×10^{16}, 3×10^{16}, and 4.5×10^{16} ions/cm^2 for implanting $\sim$1, 5, 10, and 14 at. % of Ag in PbTe, and these films will be referred to hereafter as PbTe-I:1Ag, PbTe-I:5Ag, PbTe-I:10Ag, and PbTe-I:14Ag.

Rutherford backscattering (RBS) spectrometry was performed using 2 MeV He^+ ions at a scattering angle of 165° at IUAC, New Delhi, for compositional studies. The Rutherford manipulation program (RUMP) simulation code was used to simulate the experimental RBS spectra. The surface morphology of the thin film was examined using scanning electron microscopy (SEM) by means of a TESCAN MIRA II LMH microscope. X-ray diffraction (XRD) measurements were performed at a grazing incident angle of 2° to identify the crystalline phases in the films using a Bruker D8 advance diffractometer with a Cu Kα (1.54 Å) X-ray source at a scan speed of 0.5°/min. The electrical resistivity (ρ) and thermoelectric power (S) of the films were measured in the temperature range of 300–400 K using a standard DC four probe technique and bridge method,[18] respectively. The Hall Effect measurements were carried out using a magnetic field of 0.57 T at room temperature to evaluate carrier density and mobility. The high resolution XRD measurement was carried out at the synchrotron radiation facility of KEK, Japan, using 13.9 keV. The X-ray photoelectron spectroscopy (XPS) study was performed for the elemental composition on the surface and the electronic structure of the films using a PHI 5000 Verse Probe II system and Al radiation at 100 W power at Indian Institutes of Technology, Kharagpur.

III. RESULTS

A. Compositional analysis

Figure 1 shows RBS raw data of the as-deposited and Ag-implanted PbTe films on the SiO_2 substrate. The peak position of an element in RBS is governed by its atomic number and its depth distribution. The as-deposited and implanted thin films have high atomic number elements Pb (82), Te (52), and Ag (47); therefore, their positions on the RBS spectra are quite close and as the films are thick enough, the peaks of Pb, Te, and Ag overlap each other and form a broad peak; thus, it is difficult to resolve individual peak without fitting or simulation. As a consequence of overlapping, the signals from Ag in the spectra of implanted films are not clearly noticeable. However, a close observation of the tail at the inner edge of the broad peak shows a change in the slope for implanted samples, indicating the presence of Ag atoms. In Fig. 1, the surface energies for Pb, Te, and Ag are represented by arrows, and the inset in Fig. 1 shows the spectra of pristine PbTe and PbTe-I:5Ag films. All the films were fitted using the RUMP simulation to determine the thickness of the films, atomic percent, and the depth profiling of Ag. There exist differences in thickness among the investigated samples as seen from the RBS spectra, i.e., the thickness varies from 340 nm to 360 nm. However, since the differences can hardly be correlated with the ion doses and considering that the film was deposited by thermal evaporation system in which the substrate is positioned perpendicularly to the target without substrate rotation, it is assumed that the difference in thickness exists originally in the film before implantation. However, the measured thickness of the PbTe-I:14Ag film is quite small $\sim$245 nm with respect to other implanted films because of sputtering of few atomic

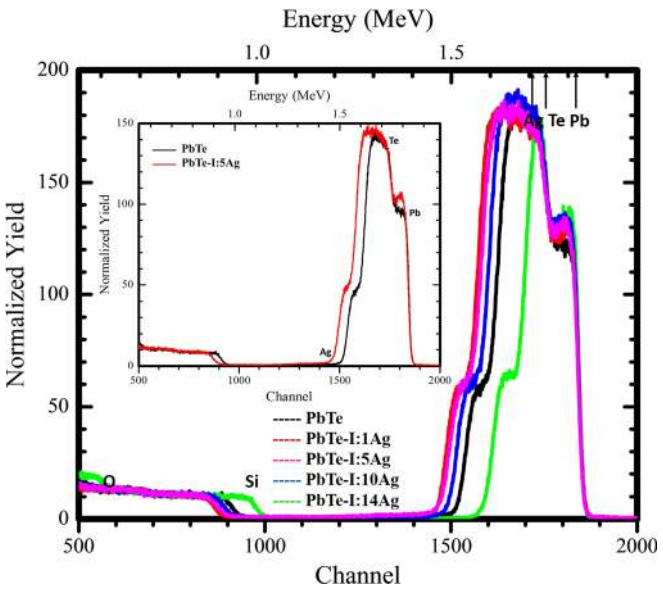

FIG. 1. RBS spectra of PbTe, PbTe-I:1Ag, PbTe-I:5Ag, PbTe-I:10Ag, and PbTe-I:14Ag thin films, and the inset shows the magnified RBS spectra of PbTe and PbTe-I:10Ag for a selected region.

layers by ion irradiation at the fluence of 4.5×10^{16} ions/cm^2. In RBS, it is difficult to present more than one spectrum along with their simulated data. Either raw data can be plotted in one graph or raw data with their simulated data. Therefore, only the raw data of PbTe and PbTe-I:5Ag films are shown in the inset of Fig. 1 and their simulated spectra are shown separately in Figs. 2(a) and 2(b). The simulation shows the presence of Ag in the PbTe-I:5Ag thin film. Using the transport of ions in matter (TRIM) simulation,[19] it is observed that the 130 keV Ag ion comes to rest at a depth of ~50 nm (ion range) in the PbTe film and forms an approximately Gaussian distribution up to a depth of ~100 nm beneath the surface due to straggling (Fig. 3). Therefore, for getting a fairly precise dopant concentrations and their distribution, the RUMP simulation has been done by dividing the film into several sublayers containing different Ag concentrations and simulating separately each layer to get the best curve fitting. The depth distribution of Ag in the PbTe film obtained from the RBS simulation for all the Ag implanted PbTe films is shown in Fig. 4(a). The unit of the y axis has been changed to the atomic fraction of Ag for a more clear representation. The peak concentrations of Ag are ~0, 1, 5, 10, and 14 at. % for the fluences 3×10^{15}, 1.5×10^{16}, 3×10^{16}, and 4.5×10^{16} ions/cm^2, respectively. At higher fluences, the sputtering is significant and hence these higher fluences are not included for further studies. The atomic density assumed for the RBS simulation for finding the thickness is Pb-3.29×10^{22} atoms/cm^3, Te-2.95×10^{22} atoms/cm^3, and Ag-5.84×10^{22} atoms/cm^3. The estimated atomic percentages of Pb, Te, Ag, and O atoms for all the films are also given in Table I. Figure 4(b) shows the theoretically

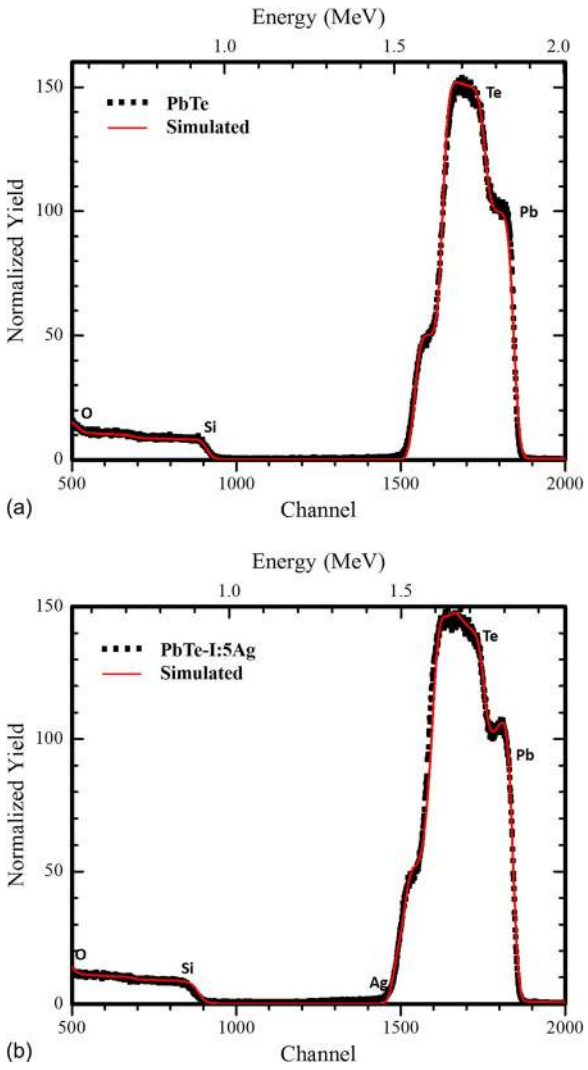

FIG. 2. RBS spectra of PbTe and PbTe-I:5Ag fitted using the RUMP simulation (black line shows the raw data and red line shows its simulation).

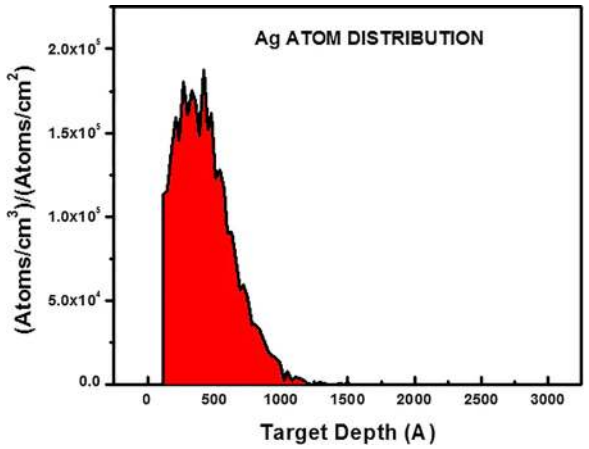

FIG. 3. TRIM simulation for atomic distribution of Ag in implanted PbTe.

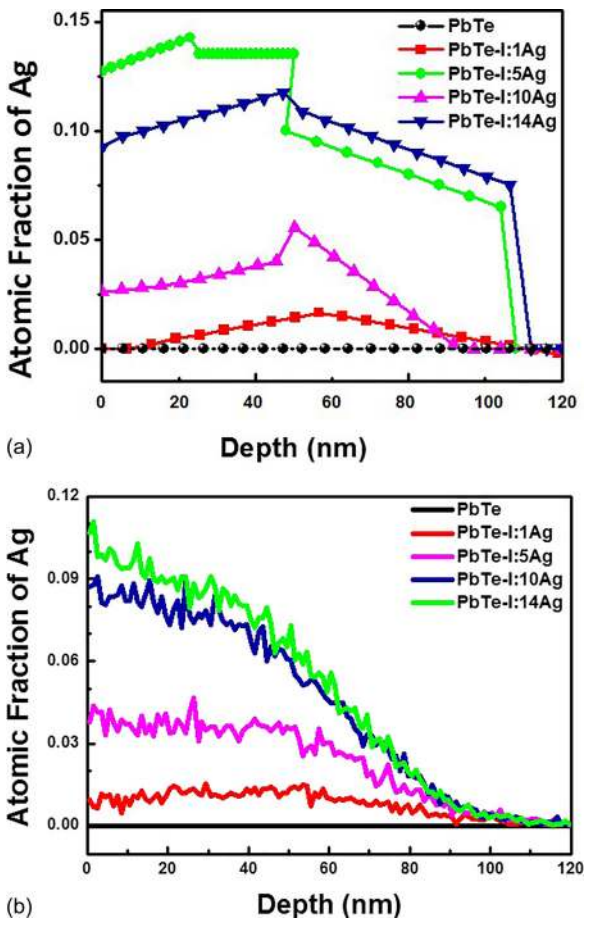

FIG. 4. Simulated depth profiles of Ag ions in PbTe, PbTe-I:1Ag, PbTe-I:5Ag, PbTe-I:10Ag, and PbTe-I:14Ag as obtained from the (a) RUMP simulation and (b)TRIDYN code.

TABLE I. Elemental compositions of PbTe, PbTe-I:1Ag, PbTe-I:5Ag, PbTe-I:10Ag, and PbTe-I:14Ag thin films for the top 100 nm film as determined by the RBS simulation.

Sample	Fluence (ions/cm^2)	Pb (at. %)	Te (at. %)	Ag (at. %)	O (at. %)
PbTe	0	40.2	41	0	18.8
PbTe-I:1Ag	3×10^{15}	40.9	41.7	1.2	16.2
PbTe-I:5Ag	1.5×10^{16}	40.7	39.9	5.4	14.0
PbTe-I:10Ag	3×10^{16}	38.1	37.8	10.7	13.4
PbTe-I:14Ag	4.5×10^{16}	37.4	35.7	14.3	12.6

calculated depth profile of Ag ions implanted in PbTe thin films by the TRIDYN code.[20] The simulation shows that the implantation depth of Ag is ∼100 nm and the maximum Ag concentrations in PbTe-I:1Ag, PbTe-I:10Ag, and PbTe-I:14Ag are 1.2 at. %, 4 at. %, 8.3 at. %, and 11.2 at. %, respectively; however, these values are less than the experimental values, which is expected because the TRIYDN simulation considers Pb and Te as individuals and not as a PbTe phase. From the TRIYDN simulation, the sputtering yields of Pb and Te decrease while that of Ag increases with ion fluence (see Fig. 5). Therefore, a further increase in the implantation fluence leads to saturation of the Ag concentration in the PbTe film.

B. Phase evolution

Figure 6 shows the Grazing Incidence X-ray Diffraction (GIXRD) patterns of PbTe, PbTe-I:1Ag, PbTe-I:5Ag, PbTe-I:10Ag, and PbTe-I:14Ag thin films. The pattern of PbTe is comparable to earlier work by Das *et al.* (*JCPDS08–0028*).[21] The high intense peak at $2\theta = 29.4°$ suggests a preferential growth along the (220) planes. The average sizes of the crystallites were determined by using the Scherrer equation. It is observed that there is no significant effect on the crystallite size which remains almost constant ∼12–13 nm for all the films after Ag ion implantation. However, an increase in peak intensity is observed after Ag ion implantation. Since the beam current of the Ag ion beam was ∼1 μA, probably the sample gets annealed and thus improves the crystal quality even though the size of crystallites did not change significantly. The GIXRD patterns obtained using lab source (Cu Kα) for Ag implanted films do not show peaks that can be assigned to Ag or its alloys with Pb-Te.

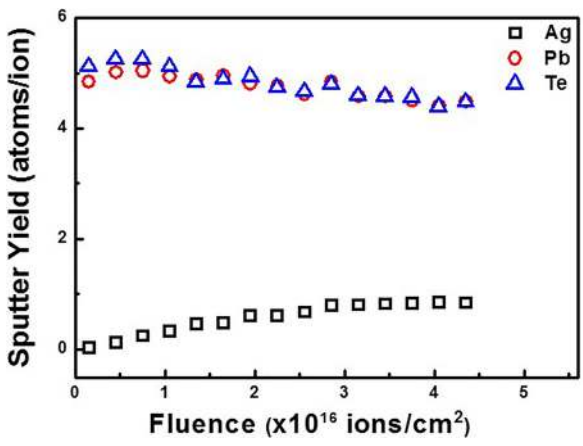

FIG. 5. Sputtering yields of Te, Pb, and Ag with fluence determined by the TRIDYN code for Ag ions.

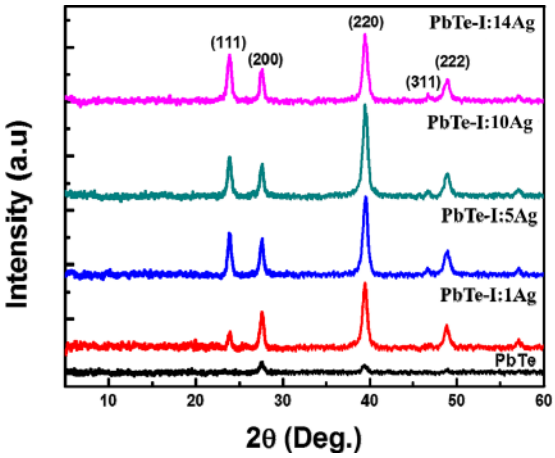

FIG. 6. XRD patterns of thin films of PbTe, PbTe-I:1Ag, PbTe-I:5Ag, PbTe-I:10Ag, and PbTe-I:14Ag.

To determine the phases present in the Ag ion implanted PbTe films, a high resolution XRD measurement was carried out at the KEK (Japan) synchrotron radiation facility using 15 keV which is capable of detecting even the small amounts of Ag and alloys of PbTe with Ag. The synchrotron XRD pattern of the PbTe-I:1Ag film showed two extra peaks at $2\theta = 21.06°$ and 23.54° (Fig. 7) which correspond to Ag_2Te (*JCPDS02–0771*) and Ag (*JCPDS75–0164*), respectively. The spectra of PbTe-I:5Ag and PbTe-I:10Ag show evolution of few more peaks assigned to Ag_2Te at 17.03°, 18.45° 19.40°, 32.84°, and 35.26° (*JCPDS04–0721*). Thus, these spectra suggest the presence of Ag and Ag_2Te phases in Ag ion implanted films. However, for PbTe-I:14Ag there is only Ag peak along with PbTe peaks and no traces of the Ag_2Te phase. This might be because at higher fluence Ag starts nucleating to form Ag clusters. The Ag-Te alloy formation was further investigated by XPS.

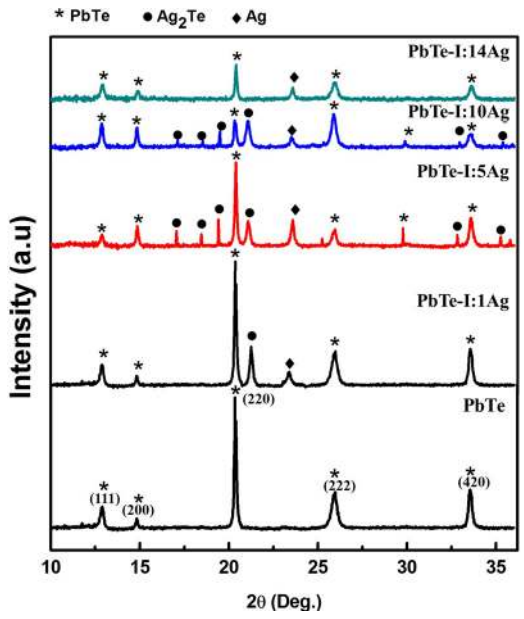

FIG. 7. Synchrotron XRD pattern of PbTe-I:1Ag, PbTe-I:5Ag, PbTe-I:10Ag, and PbTe-I:14Ag thin films.

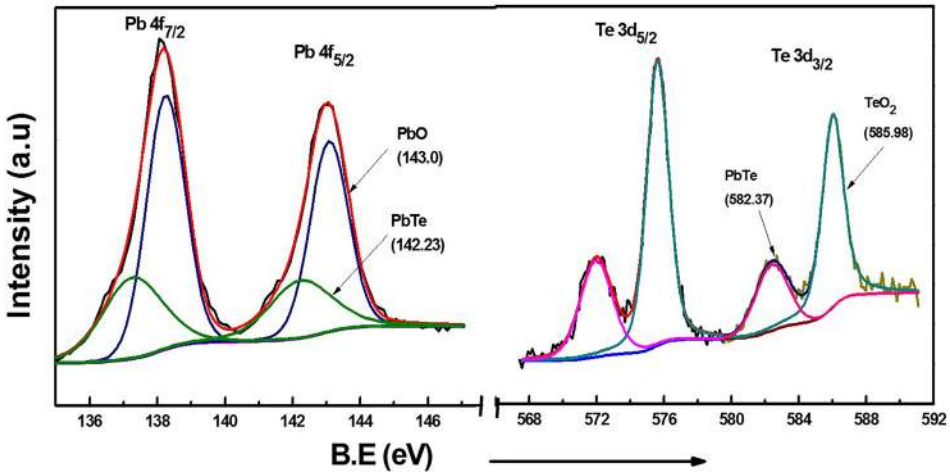

FIG. 8. XPS spectrum of PbTe showing Pb(*4f*) and Te(*3d*) peaks.

The XPS spectra of PbTe, PbTe-I:10Ag, and PbTe-I:14Ag films are shown in Figs. 8–10. For the PbTe film, the Pb ($4f_{5/2}$) peaks centered at 142.23 eV and 143.0 eV correspond to PbTe and PbO and Te ($3d_{3/2}$) peaks centered at 582.37 and 585.98 eV match with those of PbTe and TeO_2 phases (see Fig. 8). Therefore, the XPS data indicate the existence of PbO, TeO_2, and PbTe on the surface of the pristine PbTe film. The peaks for Ag appear in XPS spectra of PbTe-I:10Ag as shown in Fig. 9, and on deconvoluting, the Ag ($3d_{3/2}$) peak gives two components: 373.8 and 375.43 eV assigned to the Ag element (Ag°) and $Ag_{2-x}Te$ (Ag^{+}).[22] Although the Pb ($4f_{5/2}$) peaks of PbO and PbTe appear at the same binding energy, a shoulder peak is observed on the higher binding energy side of the Te peak. On deconvoluting the Te ($3d_{3/2}$) peak, one can distinguish two components: 581.8 eV and 583.1 eV, assigned to PbTe (Te^{2-}) and Ag_2Te

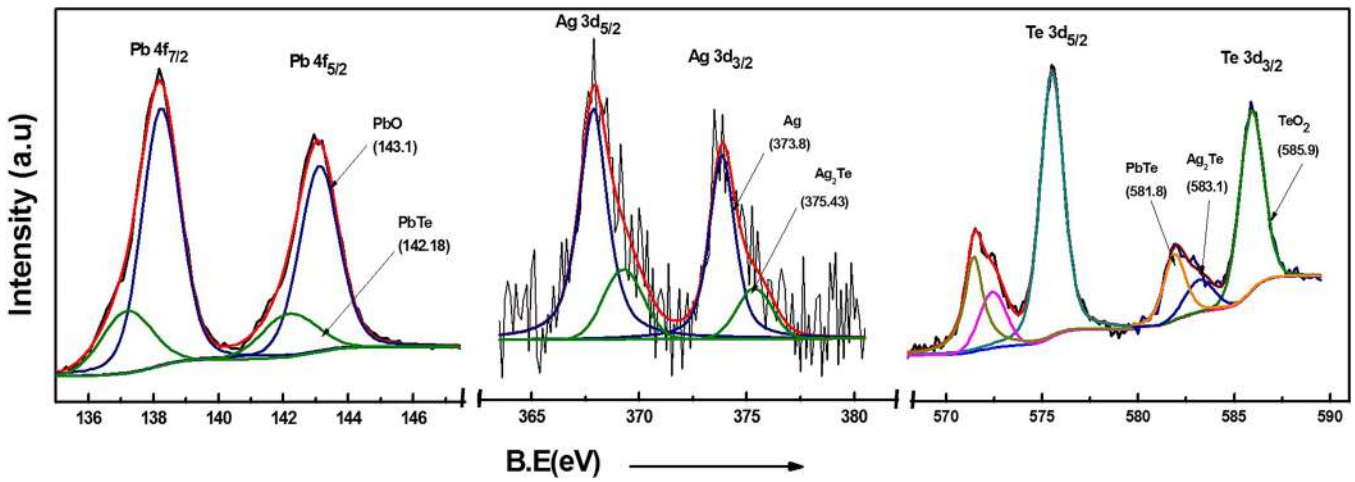

FIG. 9. XPS spectrum of PbTe-I:10Ag showing Pb(*4f*), Ag(*3d*), and Te(*3d*) peaks.

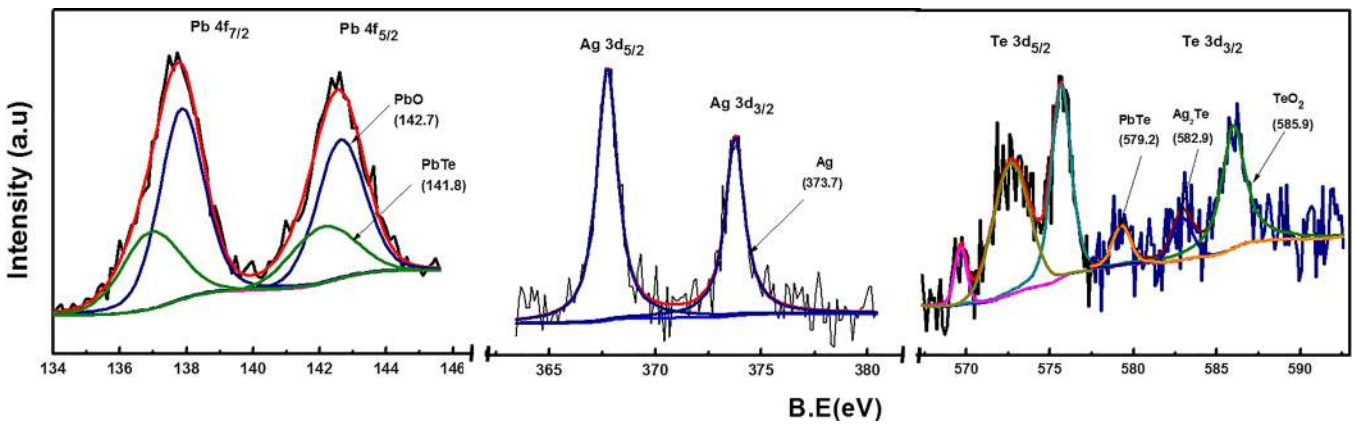

FIG. 10. XPS spectrum of PbTe-I:14Ag showing Pb(*4f*), Ag(*3d*), and Te(*3d*) peaks.

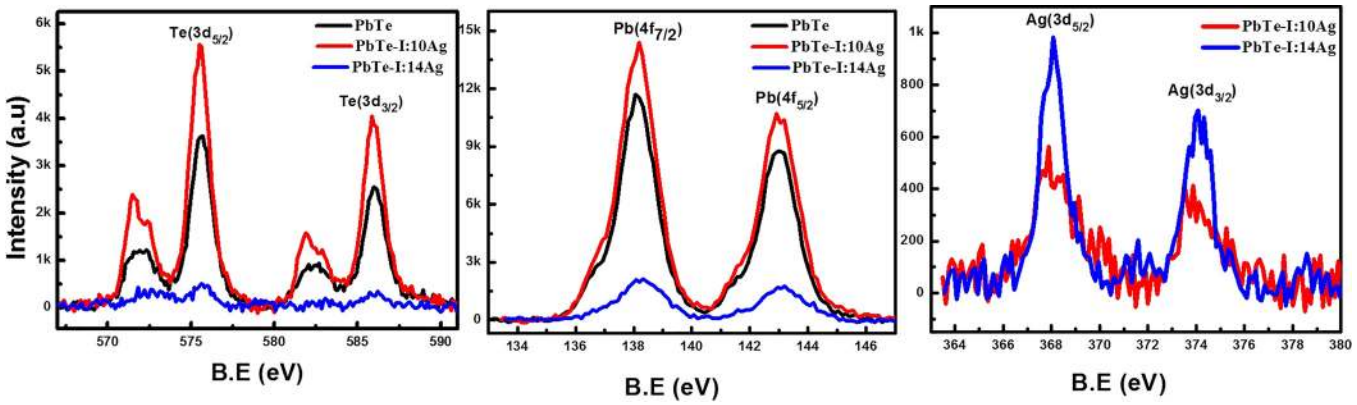

FIG. 11. Comparison of Pb 4f, Te 3d, and Ag 3d peak intensities of PbTe, PbTe-I:10Ag, PbTe-I:14Ag thin films.

(Te^{2-}), respectively. Apart from these peaks, the TeO_2 (Te^{4+}) ($3d_{3/2}$) peak also appears at 585.9 eV. The Ag peak in the spectrum of the PbTe-I:14Ag film (Fig. 10) corresponds to native Ag° and no Ag_2Te peak observed. This might be because at higher fluence (i.e., PbTe-I:14Ag) of implantation, the film contained more Ag clusters. However, on deconvolution, the Te peak indicates the presence of Ag_2Te along with PbTe and TeO_2. A shift toward lower binding energy in both Pb(*4f*) and Te(*3d*) peaks corresponding to PbTe was also observed in the PbTe-I:14Ag film. The concentration of the Ag_2Te phase has been calculated for both PbTe-I:10Ag and PbTe-I:14Ag films from the area under the XPS peak of Te(3*d*). The concentration of Ag_2Te in PbTe-I:10Ag is ∼11% and that in PbTe-I:14Ag is ∼13%, i.e., the PbTe-I:14Ag film is having 2% more Ag_2Te than the PbTe-I:10Ag film.

The peak intensities of Pb, Te, and Ag for all the films are shown in Fig. 11. The peak intensities of both Pb and Te ions are higher in the PbTe-I:10Ag film in comparison to the PbTe film. On further increasing the Ag ion fluence, the intensity of Te and Pb peaks decreases and that of Ag increases due to large sputtering of Pb and Te taking place and the formation of Ag clusters.

C. Morphological study

Figure 12 shows the surface morphology of pristine and Ag implanted PbTe thin films as examined using SEM at two different magnifications of 10 kx and 20 kx. The SEM images illustrate a significant modification of the PbTe surface after Ag ion implantation.

The fine cracks present on the surface of as-deposited PbTe thin films get shortened and suppressed on Ag implantation and finally disappeared at high fluences. This is understood on the basis of diffusion of surface atoms which tends to smoothen the surface topography. It is reported that ion implantation results in surface compressive stresses.[23,24] Lawn and Fuller[25] suggested a relationship linking the crack trace shortening to the stress acting in the surface

$$2\sigma_s \Psi d^{1/2}/K_c = 1 - (C_0/C)^{3/2},$$

where Ψ is the geometrical factor (∼1), σ_s is the surface stress, K_c is the critical stress intensity factor, C_0 is the unstressed crack length, C is the stressed crack length, and d is the thickness of the layer. For $C < C_o$, σ_s is negative, i.e., the stress is compressive. Figure 13 illustrates the change in crack length with ion fluence. The compressive stresses are

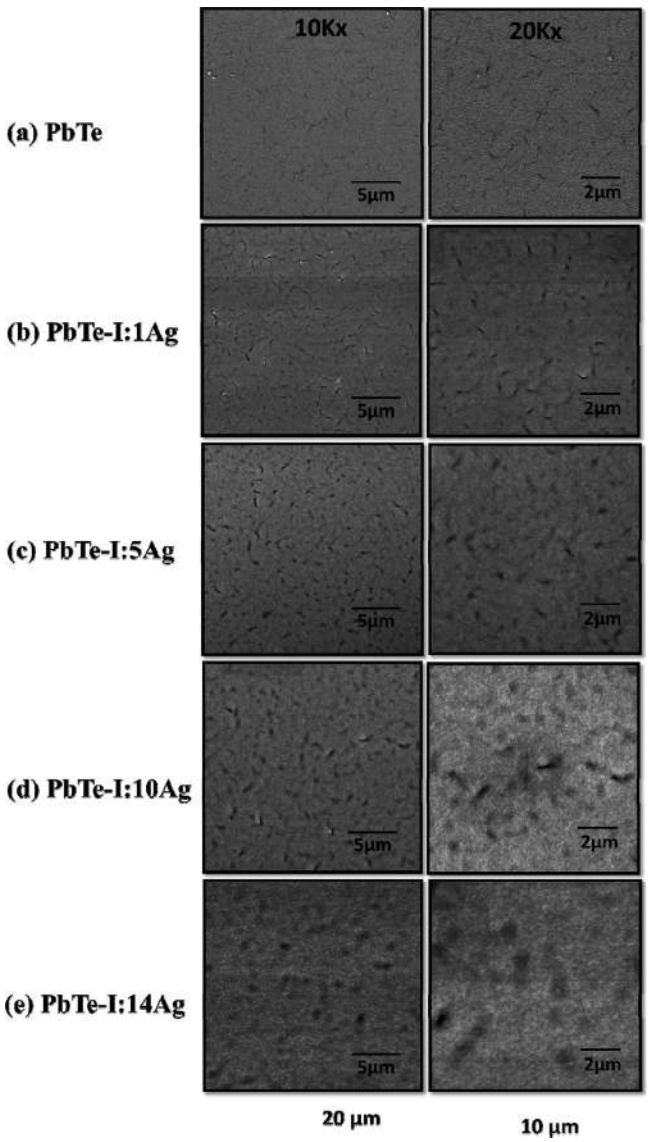

FIG. 12. SEM images of (a) PbTe, (b) PbTe-I:1Ag, (c) PbTe-I:5Ag, (d) PbTe-I:10Ag, and (e) PbTe-I:14Ag thin films.

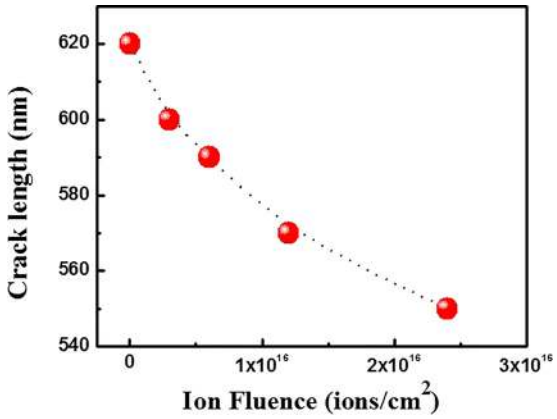

FIG. 13. Variation of crack length with ion fluence.

primarily generated by the volume expansion due to both (a) the production of vacancy/interstitial pairs (i.e., displacement damage by both the primary and knocked-on ions) and (b) the injection of large numbers of foreign atoms into the surface. The volume change within the implanted layer is constrained by either underlying or surrounding material and large stresses may be generated in this relatively thin implanted layer.[26] Since the number of defects produced is expected to be linearly dependent on ion fluence, the stresses generated are also expected to follow linear dependency with ion fluences. Defect production linearly depends on the ion fluence only at lower fluence and as the fluence increases the defects starts to annihilate. However, in the present case ion beam leads to injection of the Ag ions in the film, whose concentration increases with the ion fluences. This impurity addition in the PbTe film is also a type of defect in the homogeneous film which increases with ion fluence.

D. Electrical transport measurements

Figure 14 shows the temperature dependence of the ρ in the temperature range of 300 K to 400 K for all thin films of PbTe, PbTe-I:1Ag, PbTe-I:5Ag, PbTe-I:10Ag, and PbTe-I:14Ag. The ρ decreases constantly with Ag ion implantation of 1 at. % and 5 at. %. However, on further increasing the concentration of implantation to 10 at. % and 14 at. %, the ρ and slope of the resistivity curve increase abruptly in comparison to those of PbTe. The ρ of PbTe-I:14Ag is less than that of PbTe-I:10Ag due to the percolating effect of Ag inclusions formed at the high fluence. The change in the slope of resistivity versus temperature corresponds to the change in the temperature coefficient of resistance, $\alpha = \Delta R/(R_0 \times \Delta T)$, which depends upon material properties. Ion implantation modifies the material properties due to the impurities, dislocations, interstitial atoms, vacancies, grain boundaries, etc., and therefore the slope is expected to change. The change of the slope for PbTe-I:1Ag and PbTe-I:5Ag films is small due to the lower ion fluence; however, for PbTe-I:10Ag and PbTe-I:14Ag the change in the slope is significant due to the presence of higher Ag concentrations and different phases of Pb, Te, and Ag. The temperature dependent variations of S of all the films in the temperature range of 300 K to 400 K are shown in Fig. 15. The S of PbTe increases with Ag ion implantation up to a fluence of 3×10^{16} ions/cm^2 and on further increasing of ion fluence to 4.5×10^{16} ions/cm^2, it decreases. The measured S at 400 K for PbTe, PbTe-I:1Ag, PbTe-I:5Ag, PbTe-I:10Ag, and PbTe-I:14Ag films is ~273, ~278, ~297, ~344, and ~315 μV/K, respectively. The S of PbTe-I:10Ag and PbTe-I:14Ag thin films is found to be ~26%, and ~15% higher than that of the PbTe thin film. The S and ρ behavior can be understood on the basis of the variation in the carrier concentration, Hall mobility, and the phase formation on Ag implantation. Figure 16 shows the carrier concentration and Hall mobility for all the thin films. The carrier concentration increases with Ag ion implantation. However, the mobility of the carrier decreases with increasing fluences. This may be due the carrier scattering by dopants or the presence of some impurity phases that are not detectable by lab XRD, and or ion beam induced defects. Since the implantation depth is not exactly equal to the thickness of the films, a two-layer model for the evaluation of the Hall coefficient was used to account for the influence of the unimplanted layer.[27,28] This

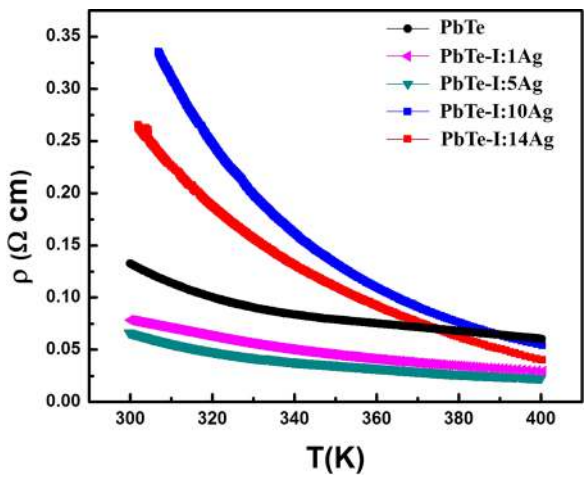

FIG. 14. Electrical resistivities of PbTe, PbTe-I:1Ag, PbTe-I:5Ag, PbTe-I:10Ag, and PbTe-I:14Ag thin films in the temperature range of 300 K–400 K.

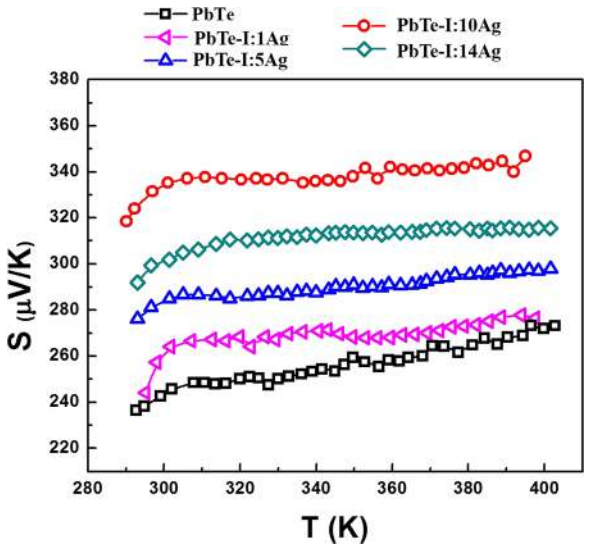

FIG. 15. Thermoelectric powers of PbTe, PbTe-I:1Ag, PbTe-I:5Ag, PbTe-I:10Ag, and PbTe-I:14Ag thin films in the temperature range of 300 K–400 K.

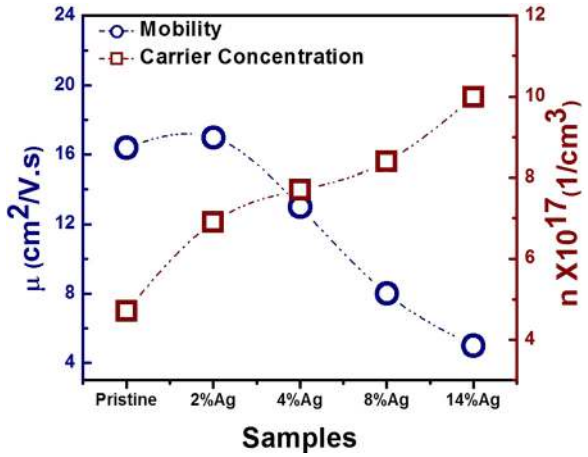

FIG. 16. Carrier mobility and concentration of PbTe, PbTe-I:1Ag, PbTe-I:10Ag, and PbTe-I:14Ag.

correction is relatively small for the reasons that the carrier concentration in the damaged region is much higher than in the undamaged region.[29]

IV. DISCUSSION

Synchrotron XRD and XPS investigations confirmed that Ag ion implantation results in the formation of the Ag_2Te phase in the PbTe thin film and the concentration of Ag_2Te increases with Ag ion fluence up to 10 at. % Ag concentration, i.e., PbTe-I:10Ag. With still higher Ag concentrations, i.e., PbTe-I:14Ag, there is a formation of Ag clusters. It is known from the previous studies[8,12] that Ag ions preferentially bind with Te by liberating Pb atoms to precipitate out. In the present study, however, no extra peak corresponding to Pb is observed in the XRD spectra of the implanted PbTe samples. This may possibly be because PbO in amorphous form cannot be detected by XRD or it is present at the grain boundaries.

The surface of the pristine PbTe thin film has cracks on the surface and the measured resistivity of this sample is 0.12 Ω cm. This value is 10 times higher than the value reported for crack free PbTe thin films.[10,12] When the as-prepared films were implanted with Ag ions, the ρ decreases constantly for 1 at. % and 5 at. % due to suppression of surface cracks with ion fluences. On further increasing the concentration to 10 at. % and 14 at. %, the surface gets more smoothen. However, the ρ increases abruptly due to the impurities, vacancies, and defects created in the PbTe films at high fluences. The higher ρ of PbTe-I:10Ag is also because of the formation of more and more Ag_2Te alloy liberating Pb out and hence distorting the lattice. The ρ of PbTe-I:14Ag is less than that of PbTe-I:10Ag either due to the percolating effect of Ag inclusions formed at such a high fluence which increased the carrier concentration and hence decrease the ρ of this films or/and due to smoothening of all the surface cracks. The S is the highest for the PbTe-I:10Ag film due to the formation of the Ag_2Te nanocomposite whereas for PbTe-I:14Ag, it decreases due to the formation of Ag inclusions which provides a percolation path for the charge carriers and hence decreases ρ and S. The charge scattering due to grain boundaries or due to impurity scattering may also have probably increased the S.[9,30] Therefore, the S increases with Ag implantation up to a concentration of 10 at. % Ag and then decreases on further increasing the Ag concentration to 14 at. % due to the percolation effect from Ag inclusions.

The surface oxidation of PbTe takes place very easily on exposure to air. The chemisorption of oxygen essentially forms carrier trapping acceptor states by removing electrons from the grain surface, reducing itinerant carrier density. For nanocrystalline materials, this chemisorption increases the trapping of carriers at grain boundaries leading to the formation of energy barriers that impede the conduction of carriers between grains. These results are in agreement with earlier reports, suggesting that the electrical resistivity of PbTe can increase up to 2 to 3 orders of magnitude after exposing to air.[19] Thus, the formation of carrier trapping acceptor states with the oxidation of PbTe is responsible for the low energy carrier filtering which enhances the S.[31]

Some work has also been reported on the effect of Ag addition in PbTe during thin film deposition.[12,19] PbTe films grown with Ag form rice like nanostructures on the surface. This nanostructuring improves thermoelectric power by ~30% for 10 at. % Ag added PbTe in comparison with the pristine PbTe thin film. Synchrotron based X-ray diffraction and XPS were performed to confirm the phases of Ag alloys, which show the formation of $Ag_{2-x}Te$ and precipitation of Pb on the surface of Ag added PbTe films. For the Ag ion implanted PbTe thin films, Ag_2Te phases are observed; however, there were no nanostructures of Pb on the surface; for higher implantation fluence of Ag, there was formation of Ag clusters. The maximum S for the 10 at. % Ag implanted PbTe thin film is 344 μV/K which is ~25% higher than the pristine PbTe thin film. The maximum value of S for the implanted sample is however less than the value reported for Ag added PbTe thin films due to the absence of surface nanostructuring by Pb and presence of large defects due to the implantation process. The mechanism of defect generation can be understood as follows. Ag ions come to rest in an approximately Gaussian distribution in PbTe. In addition to the solute profile so-introduced, the incoming Ag ions also leave a trail of damage as these penetrate the material. During ion implantation, two major classes of defects are introduced, namely, the implanted ions themselves and radiation damage (e.g., interstitial/vacancy pairs). The latter defects arise as a result of displacements occurring in response to "knock-on" collisions. These displacements may be caused both by the incident ions themselves (primary collisions) and by other "knocked-on" atoms (secondary collisions). It is reasonable to assume that a collision cascade results in a highly disordered region surrounded by point defects.[27,32] The number of initial collisions results in electrically active defects (donors) and the number of such defects increases with fluences.

V. CONCLUSION

The nanostructured PbTe:Ag composite thin films were fabricated on PbTe by Ag ion implantation with 1 at. %, 5 at.

%, 10 at. %, and 14 at. %. Maximum thermoelectric power was observed for 10 at. % Ag implanted PbTe thin films and was found to be ~25% higher than the pristine PbTe thin film. The XRD measurement from synchrotron source and the XPS were performed to confirm the phases of the Pb-Ag-Te alloy which show the formation of $Ag_{2-x}Te$ and precipitation of PbO on the surface of Ag implanted PbTe films. The XPS measurements suggest the presence of the Ag_2Te phase in the Ag implanted PbTe thin films. However, for higher Ag concentrations there was formation of Ag clusters. Therefore, the increase in thermoelectric power with increasing Ag ion fluence can be attributed to the formation of the Ag_2Te phase.

ACKNOWLEDGMENTS

One of the authors Manju Bala is grateful to the Council for Scientific and Industrial Research (CSIR) for providing financial support in the form of fellowship. The authors would like to thank Mrs. Devarani Kshetri and Mr. Sunil Ojha for their help in carrying out ion implantation and RBS measurement and discussion. The authors thank Ms. Jagdish, Panjab University, Chandigarh, for sample preparation, Dr. S. K. Srivastava, IIT Kharagpur, for XPS measurements, and Dr. M. Posselt of Helmholtz Zentrum Rossendorf (Dresden, Germany) for providing the TRIDYN simulation code.

[1]J. F. Gibbons, "Ion implantation in semiconductors—Part II: Damage production and annealing," Proc. IEEE **60**(9), 1062–1096 (1972).
[2]H. Goldsmid and R. Douglas, "The use of semiconductors in thermoelectric refrigeration," Br. J. Appl. Phys. **5**(11), 386 (1954).
[3]J. F. Ziegler and J. P. Biersack, "The stopping and range of ions in matter," in *Treatise on Heavy-Ion Science* (Springer, 1985), pp. 93–129.
[4]D. Kraemer *et al.*, "High-performance flat-panel solar thermoelectric generators with high thermal concentration," Nat. Mater. **10**(7), 532–538 (2011).
[5]M. Komabayashi, K-i. Hijikata, and S. Ido, "Effects of some additives on thermoelectric properties of $FeSi_2$ thin films," Jpn. J. Appl. Phys., Part 1 **30**(2R), 331 (1991).
[6]G. J. Snyder and E. S. Toberer, "Complex thermoelectric materials," Nat. Mater. **7**(2), 105–114 (2008).
[7]J. P. Heremans *et al.*, "Enhancement of thermoelectric efficiency in PbTe by distortion of the electronic density of states," Science **321**(5888), 554–557 (2008).
[8]J. P. Heremans, C. M. Thrush, and D. T. Morelli, "Thermopower enhancement in PbTe with Pb precipitates," J. Appl. Phys. **98**(6), 063703 (2005).
[9]J. Martin *et al.*, "Enhanced Seebeck coefficient through energy-barrier scattering in PbTe nanocomposites," Phys. Rev. B **79**(11), 115311 (2009).
[10]H. Dow *et al.*, "Effect of Ag or Sb addition on the thermoelectric properties of PbTe," J. Appl. Phys. **108**(11), 113709 (2010).
[11]B. Paul, A. Kumar, and P. Banerji, "Embedded Ag-rich nanodots in PbTe: Enhancement of thermoelectric properties through energy filtering of the carriers," J. Appl. Phys. **108**(6), 064322 (2010).
[12]M. Bala *et al.*, "Enhancement of thermoelectric power of PbTe: Ag nanocomposite thin films," RSC Adv. **5**(33), 25887–25895 (2015).
[13]K. Biswas *et al.*, "Strained endotaxial nanostructures with high thermoelectric figure of merit," Nat. Chem. **3**(2), 160–166 (2011).
[14]K. Biswas *et al.*, "High-performance bulk thermoelectrics with all-scale hierarchical architectures," Nature **489**(7416), 414–418 (2012).
[15]Q. Shen, J. Li, and L. Zhang, "A study on Sn ion implantation into lead telluride thermoelectric material," Sol. Energy Mater. Sol. Cells **62**(1), 167–172 (2000).
[16]Y. Kato *et al.*, "p-n junction formation by Te^+ ion implantation into solution-grown $Pb_{1-x}Sn_xTe$," J. Appl. Phys. **46**(10), 4614–4615 (1975).
[17]J. Donnelly *et al.*, "p-n junction photodiodes in PbTe prepared by Sb^+ ion implantation," Appl. Phys. Lett. **20**(8), 279–281 (1972).
[18]T. Tripathi, M. Bala, and K. Asokan, "An experimental setup for the simultaneous measurement of thermoelectric power of two samples from 77 K to 500 K," Rev. Sci. Instrum. **85**(8), 085115 (2014).
[19]J. F. Ziegler, M. D. Ziegler, and J. P. Biersack, "SRIM–The stopping and range of ions in matter (2010)," Nucl. Instrum. Methods Phys. Res., Sect. B **268**(11), 1818–1823 (2010).
[20]W. Möller and W. Eckstein, "Tridyn—A TRIM simulation code including dynamic composition changes," Nucl. Instrum. Methods Phys. Res., Sect. B **2**(1), 814–818 (1984).
[21]V. D. Das and K. S. Bhat, "Electrical conductivity of air-exposed and unexposed lead telluride thin films-temperature and size effects," J. Phys. D: Appl. Phys. **22**(1), 162 (1989).
[22]A. Samal and T. Pradeep, "Room-temperature chemical synthesis of silver telluride nanowires," J. Phys. Chem. C **113**(31), 13539–13544 (2009).
[23]P. Burnett and T. Page, "Criteria for mechanical property modifications of ceramic surfaces by ion implantation," Radiat. Effects **97**(3–4), 283–296 (1986).
[24]P. Burnett and T. F. Page, "An investigation of ion implantation-induced near-surface stresses and their effects in sapphire and glass," J. Mater. Sci. **20**(12), 4624–4646 (1985).
[25]B. R. Lawn and E. R. Fuller, Jr., "Measurement of thin-layer surface stresses by indentation fracture," J. Mater. Sci. **19**(12), 4061–4067 (1984).
[26]G. Krefft and E. EerNisse, "Volume expansion and annealing compaction of ion-bombarded single-crystal and polycrystalline α-Al_2O_3," J. Appl. Phys. **49**(5), 2725–2730 (1978).
[27]L. Palmetshofer *et al.*, "Ion-implantation-induced lattice defects in PbTe," Appl. Phys. Lett. **30**(11), 557–559 (1977).
[28]H. Heinrich *et al.*, "Lattice defects in semiconductors 1974," in Inst. Phys. Conf. Ser. **23**, 1 (1975).
[29]L. Palmetshofer *et al.*, "Evaluation of doping profiles in ion-implanted PbTe," J. Appl. Phys. **49**(3), 1128–1130 (1978).
[30]A. Popescu *et al.*, "Model of transport properties of thermoelectric nanocomposite materials," Phys. Rev. B **79**(20), 205302 (2009).
[31]D. E. Bode and H. Levinstein, "Effect of oxygen on the electrical properties of lead telluride films," Phys. Rev. **96**(2), 259 (1954).
[32]J.-F. Morhange, R. Beserman, and J. C. Bourgoin, "Study of defects introduced by ion implantation in diamond," Jpn. J. Appl. Phys. **14**(4), 544 (1975).